

INVESTIGATION OF THE INTERFACIAL HEAT TRANSFER COEFFICIENT AT THE METAL–MOLD INTERFACE DURING CASTING OF AN A356 ALUMINUM ALLOY AND AZ81 MAGNESIUM ALLOY INTO STEEL AND GRAPHITE MOLDS

V. E. Bazhenov , Yu. V. Tselovalnik, A. V. Kolytgin, and V. D. Belov

Foundry Department, National University of Science and Technology (MISiS), Leninskiy Pr. 4, Moscow, Russia 119049

Copyright © 2020 American Foundry Society
<https://doi.org/10.1007/s40962-020-00495-2>

Abstract

Many types of alloys can be cast in graphite molds. The advantage of using graphite molds is that graphite has a higher thermal conductivity than steel and provides a higher alloy cooling rate. In this work, the solidification conditions in graphite and steel molds are compared. Cylindrical ingots of A356 aluminum and AZ81 magnesium alloys were cast into steel and graphite molds, and the temperature was recorded by thermocouples positioned in both the ingots and the molds. Using the error function, which is a measure of the difference between the experimental and simulated temperatures, the interfacial heat transfer coefficient (IHTC) versus the ingot surface temperature curves were obtained. The peak IHTC for ingot

casting in the graphite mold was 2–3 times higher than that for the steel mold for both alloys. The solidification time and cooling rate for the solidification of the A356 and AZ81 ingots with varied sizes in the graphite and steel molds were calculated based on the simulation results. The duration of the solidification process in the steel mold was nearly two times longer than that for ingots in the graphite mold. The cooling rate in the graphite mold was nearly 1.5–2 times higher than that in the steel molds.

Keywords: computer simulation, ProCast, IHTC, graphite mold, steel mold, cooling rate

Introduction

Steel is one of the materials commonly used for permanent mold production in casting practice. However, mold materials that promote an increased cooling rate are sometimes needed to improve the mechanical properties of ingots.¹ For example, graphite molds are suitable for casting ingots that are subsequently deformation processed.^{2,3} Since graphite has a higher thermal conductivity than steel, graphite molds allow a higher cooling rate during the casting process. Titanium, nickel, copper, aluminum, and zinc castings are produced using graphite molds.^{4–11} The most promising technique is casting into a permanent graphite mold, in which a mold is produced by CNC milling of a graphite block.¹² If the strength of a graphite mold is insufficient, a graphite lining can be used in permanent steel molds.¹³ The technological advantage when graphite is used as a mold material is that no die coatings or lubricants are needed, in contrast to the situation for a steel mold, since graphite is a solid lubricant.¹¹

This work quantifies the differences between the cooling rates of permanent molds made of graphite and steel using casting process simulation. For computer simulations of casting processes, the thermal properties of the alloy and the mold need to be known. In addition, the interfacial heat transfer coefficient (IHTC) is also needed. The IHTC depends on many parameters^{14–22} and is usually obtained experimentally. In most works, experimental IHTC versus time^{15,18,23–27} or IHTC versus ingot surface temperature curves were obtained.^{16,23,24} The first is not appropriate for casting simulation, and it can be used only for castings with the same shape. Because of that, the IHTC versus ingot surface temperature dependence was chosen in this investigation.

In a considerable number of works, the IHTC at aluminum alloy/steel mold interfaces can be found. The peak IHTC varies from 1300 to 3000 W m⁻² K⁻¹.^{28–32} For aluminum alloy/graphite, the maximum IHTC ranges from 1800 to 4700 W m⁻² K⁻¹, depending on the coating used in the experiment.³³ No information is available about the IHTC

between magnesium alloys and graphite molds in the literature, but the peak value of the IHTC at an AZ91/steel mold interface was determined to be $2930 \text{ W m}^{-2} \text{ K}^{-1}$.³⁴ The IHTC in the case of a graphite mold casting is higher than that for a steel mold casting.

Reasons for the observed discrepancies in the IHTC include variations in the roughness of the mold, different alloy compositions, and melt superheating.^{29,35} Thus, the IHTC should be compared under similar casting conditions. Therefore, to compare cooling rates during ingot casting in graphite and steel molds, the IHTCs for the alloy/mold interfaces needs to be obtained first.

Materials and Methods

Melt Preparation

The A356 aluminum alloy was melted in a clay graphite crucible. The raw materials were aluminum (99.99 wt% purity), magnesium (99.9 wt%), and an Al-12 wt% Si master alloy. The AZ81 magnesium alloy was melted in a steel crucible under a cover of carnallite flux ($\text{KCl} \cdot \text{MgCl}_2$). To prepare the AZ81 alloy, magnesium (99.9 wt% purity), aluminum (99.99 wt%), zinc (99.98 wt%), and the Al-10 wt% Mn master alloy were used. The melting of both alloys was carried out in a 20 kHz induction furnace.

The composition of the A356 aluminum alloy was determined using a Bruker Q4 Tasman optical emission spectrometer. To determine the chemical composition of the AZ81 magnesium alloy, a Tescan Vega SBH3 scanning electron microscope equipped with an Oxford energy-dispersive X-ray spectroscopy analysis system was used. Areas with dimensions of $1 \times 1 \text{ mm}$ were analyzed. The chemical compositions of the alloys are presented in Table 1, and their compositions were within the limits of the A356 and AZ81 alloys.³⁶

Ingot Casting with Thermal Profile Recording

First, the A356 aluminum and AZ81 magnesium alloys were poured into molds made from 1015 grade steel. For both alloys, the pouring temperature of the melt was $720 \text{ }^\circ\text{C}$. The ingots were 35 mm in diameter and 140 mm in height. The mold wall thickness was 22 mm, and no die coating was used. Four holes with a diameter of 2 mm were drilled into the outer wall of the mold, and K-type thermocouples were fixed in the holes using a hot adhesive. The holes were drilled to various depths in the wall so that the distances from the inner mold surface to the hot ends of the thermocouples were 2, 5, 10, and 15 mm. The steel mold and the positions of the thermocouples are shown in

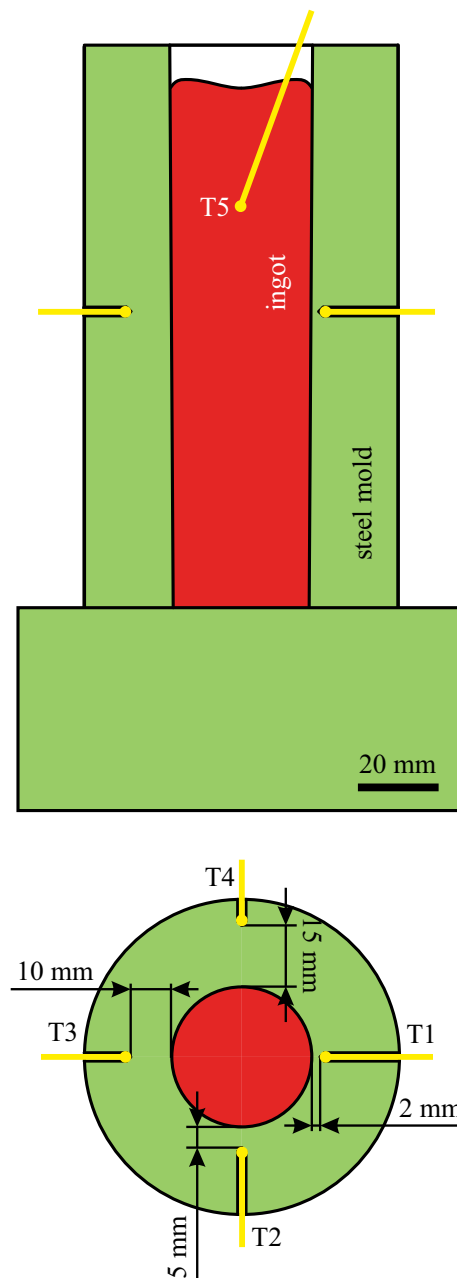


Figure 1. The steel mold and thermocouple positions.

Table 1. Chemical Compositions of Ingots

Alloy/mold couple	Content of each component of the alloy (wt%)				
	Al	Mg	Si	Zn	Mn
A356/steel	Balance	0.50	7.20	–	–
A356/graphite	Balance	0.38	7.41	–	–
AZ81/steel	7.65	Balance	–	0.76	0.19
AZ81/graphite	8.08	Balance	–	0.75	0.27

Figure 1. One of the thermocouples (T5) was placed into the mold cavity to measure the temperature of the ingot.

Next, ingots comprising A356 and AZ81 alloys that were 50 mm in diameter and 100 mm in height were cast into molds made from GMZ grade graphite (Russia). The mold was CNC milled from graphite blocks. The mold and positions of the thermocouples are shown in Figure 2. The mold wall thickness ranged from 75 to 115 mm. A die coating was not applied. The thermocouples were positioned at two different heights. Thermocouples T1–T5 were at the lower level, and thermocouples T6–T9 were at the higher level. The distances from the inner surface of the mold to the hot ends of the thermocouples were 2, 5, 10,

and 20 mm for both levels. Thermocouple T5 was inserted into an alumina tube and placed in the mold cavity 10 mm beyond the inner surface of the mold. After the alloys were poured, the temperature was recorded using a Lutron BTM-4208SD 12-channel temperature recorder with a frequency of 1 s.

A Marsurf M 300C surface roughness tester is used to measure the roughness of the inner mold surface that contacted the alloy. It is known that during mold using the roughness can change and because of that the roughness measured after experiments was ended.³⁷ The inner mold surface roughness of the steel and graphite molds was the same ($R_z = 25 \mu\text{m}$ or $R_a = 4 \mu\text{m}$).

Simulation and Determination of the IHTCs

The commercial software ProCast 2018 was used to simulate the filling of the molds and the solidification of the ingots. For the heat flow calculation, the Fourier heat conduction equation was solved, and for the mold filling calculation, the Navier–Stokes equation was solved. A finite-element method was used to solve the equations in ProCast. A Newtonian viscosity model with momentum-dominated movement of the free surface and the mass conservation contribution algorithm were used.³⁸ Details of the calculations and equations can be found in Refs. 39–41.

The temperature dependences of the thermal conductivity, enthalpy, density, and solid fraction, as well as the alloy liquidus and solidus temperatures, for the A356 aluminum alloy, the AZ81 magnesium alloy, and 1015 steel were calculated using the thermodynamic database in ProCast. The thermal properties of MPG-6 grade graphite (Russia) from Ref. 42 were used in the simulation of graphite mold casting.

The filling time observed for the steel mold in the experiments and used for simulation was 6 s, and that for the graphite mold was 3 s. The initial alloy and mold temperatures were 720 °C and 25 °C, respectively. The previously determined IHTC between mold parts (graphite/graphite) of $1000 \text{ Wm}^{-2}\text{K}^{-1}$ were used.⁴³ Additionally, the IHTC for graphite/air, steel/air, and alloy/air pairs was set as $10 \text{ Wm}^{-2}\text{K}^{-1}$ in accordance with ProCast database recommendations. The accuracy of the IHTC for that pair was confirmed previously.⁴³

The simulated ingot and mold temperatures for different IHTC values were compared to the measured temperatures through a trial-and-error process. The IHTC was fitted to minimize T^{Err} in accordance with the flowchart shown in Figure 3. The error function T^{Err} , which is a measure of the difference between the experimental and calculated temperatures for both the mold and ingot during pouring, solidification, and cooling, is:²⁴

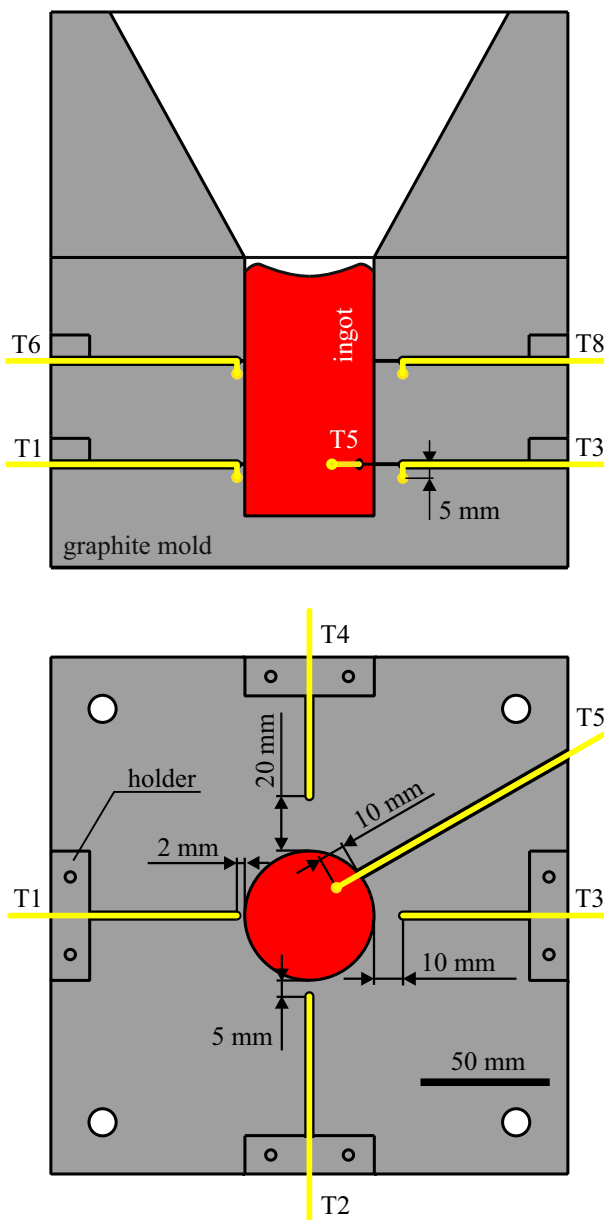


Figure 2. The graphite mold and thermocouple positions.

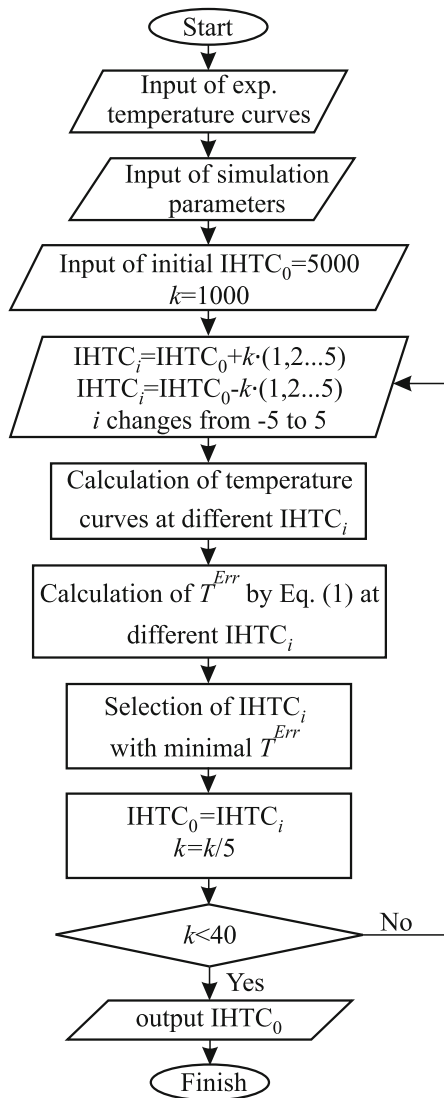


Figure 3. Fitting IHTC procedure.

$$T^{Err} = \sqrt{\sum_{j=1}^n \sum_{i=1}^m (T_{ij}^{exp} - T_{ij}^{sim})^2 / nm} \quad \text{Eqn. 1}$$

where T_{ij}^{exp} is the experimentally measured temperature at time i for thermocouple j , T_{ij}^{sim} is the same but obtained by simulation, n is the total number of time points, and m is the number of thermocouples.

Calculation of the Solidification Times and Cooling Rates for Steel and Graphite Mold Castings

We used a simulation of the ingot casting to compare the solidification times and cooling rates during solidification of the alloys in the cylindrical steel and graphite molds.

The diameter of the ingots, D , was changed from 10 to 100 mm in steps of 10 mm. The ingots for both alloys had a height of $2D$ and a wall thickness of $D/2$. The IHTC versus temperature curves found in this work were used as boundary conditions. The cooling rate over the solidification range was calculated as the average for thermocouples T1–T6, and the positions in the ingot are shown in Figure 4.

Results and Discussion

Analysis of Alloy and Mold Material Thermal Properties

Figure 5 compares the thermal properties calculated by ProCast with those from the literature.^{44–55} In ProCast, the heat capacity of alloys cannot be calculated. The enthalpy calculated in ProCast was used for the A356 aluminum alloy and 1015 steel heat capacity calculations. The calculated density, thermal conductivity, and heat capacity for a wide range of temperatures for 1015 steel are close to those in the literature for 1008, 1015, and 1020 steels. However, the thermal conductivity and heat capacity in the ProCast database for graphite are far from those given in

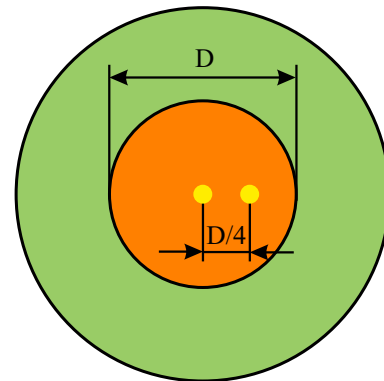
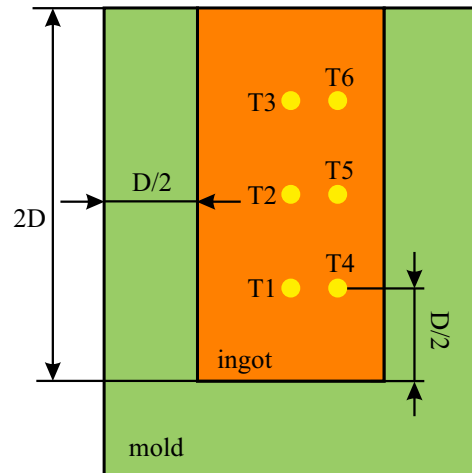


Figure 4. The ingot and mold used in the cooling rate and solidification time simulation.

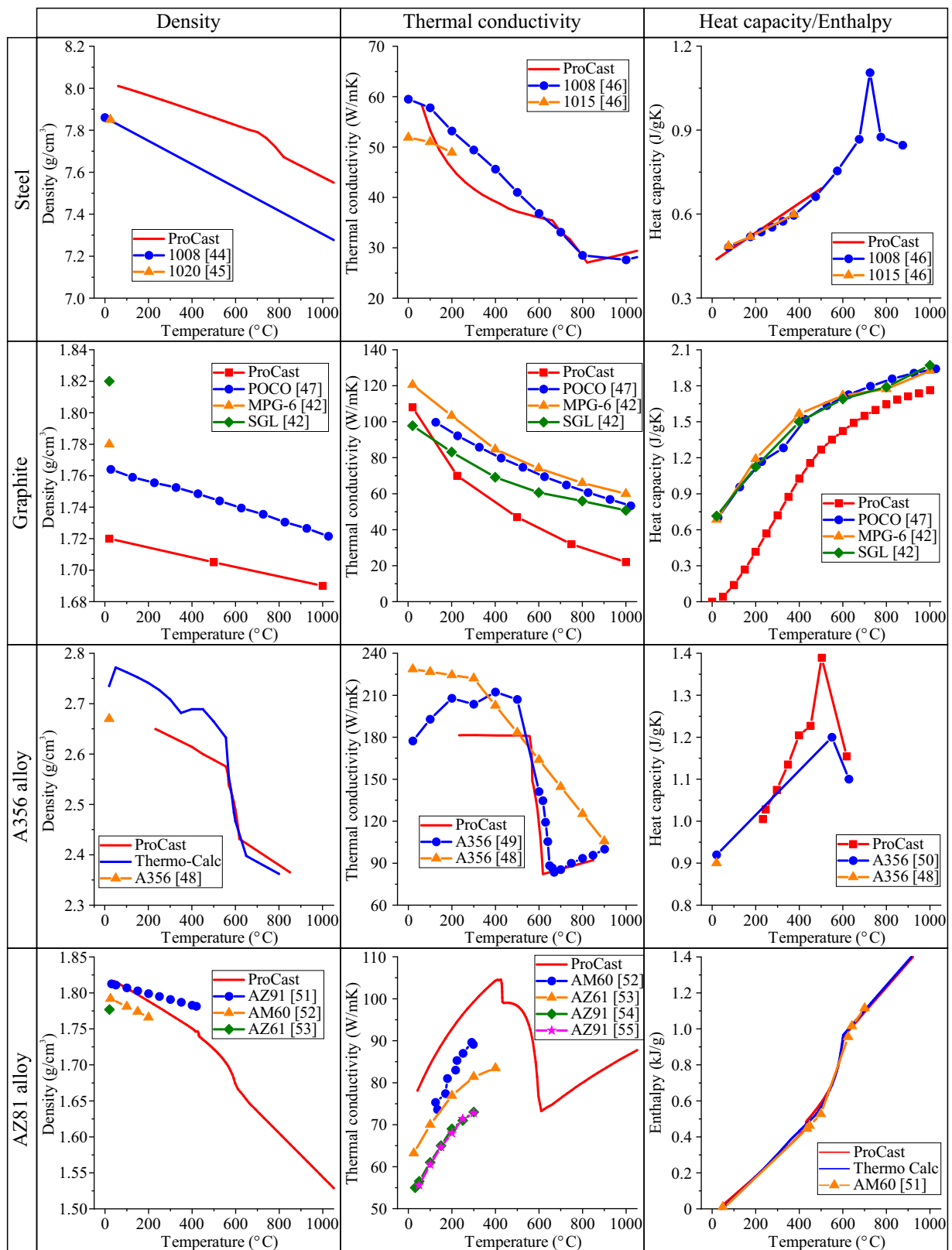


Figure 5. The thermal properties (density, thermal conductivity, heat capacity, and enthalpy) calculated in ProCast and given in the literature for the materials used for the alloys and the molds and for similar materials.

the literature. Thus, the experimentally obtained graphite thermal properties were used.⁴²

The calculated densities and heat capacities of the A356 aluminum alloy are close to those in the references. Good agreement between the calculated ProCast thermal conductivity and the experimental thermal conductivity is presented in Ref. 49. The thermal conductivity presented in Ref. 48 differs from the calculated results and data presented in Ref. 49, but these results (Ref. 48) may be wrong because no sharp change in the thermal conductivity over the solidification range was observed.

A good fit was observed between the density and enthalpy values calculated for the AZ81 magnesium alloy and those experimentally obtained for other Mg–Al–Zn–(Mn) alloys (AZ91, AZ61, and AM60). The enthalpy of AZ81 was calculated using Thermo-Calc software, and good agreement was observed. The calculated thermal conductivity for the AZ81 alloy is slightly higher than those for other magnesium alloys in the references, but this discrepancy was not critical.

The calculated thermal properties of alloys and mold materials are in good agreement with those obtained experimentally and presented in the literature. This is not surprising when using available alloys and mold materials. Because the calculated thermal properties were subsequently used, a complicated procedure for experimental thermal property determination was not needed.

IHTC vs. Temperature Curves

Figure 6a shows that the IHTC between the steel mold and the A356 aluminum alloy increased as the alloy temperature decreased from the pouring temperature to a temperature close to the liquidus. The peak IHTC was $2050 \text{ W m}^{-2} \text{ K}^{-1}$ at 640°C (near the A356 alloy liquidus temperature of 613°C). Then, due to solid skin shrinkage during solidification, the IHTC decreased to $600 \text{ W m}^{-2} \text{ K}^{-1}$. When the surface temperature of the ingot was below 400°C , the IHTC was $200\text{--}250 \text{ W m}^{-2} \text{ K}^{-1}$. In Ref. 32 and Ref. 31, the peak IHTC values were 2600 and $1700 \text{ W m}^{-2} \text{ K}^{-1}$, respectively, which is close to that found in our work.

The trends for the IHTC for the A356 aluminum alloy and graphite mold are the same as those for the A356/steel pair. When the ingot surface temperature was near the A356 alloy liquidus temperature (613°C), a peak IHTC of $4700 \text{ W m}^{-2} \text{ K}^{-1}$ was observed. This value is in the range of A356/graphite peak IHTC from 1800 to $4700 \text{ W m}^{-2} \text{ K}^{-1}$ presented in the literature.³³ When the ingot surface temperature was lower than 400°C , the IHTC for the A356/graphite pair was nearly the same as that for the A356/steel pair.

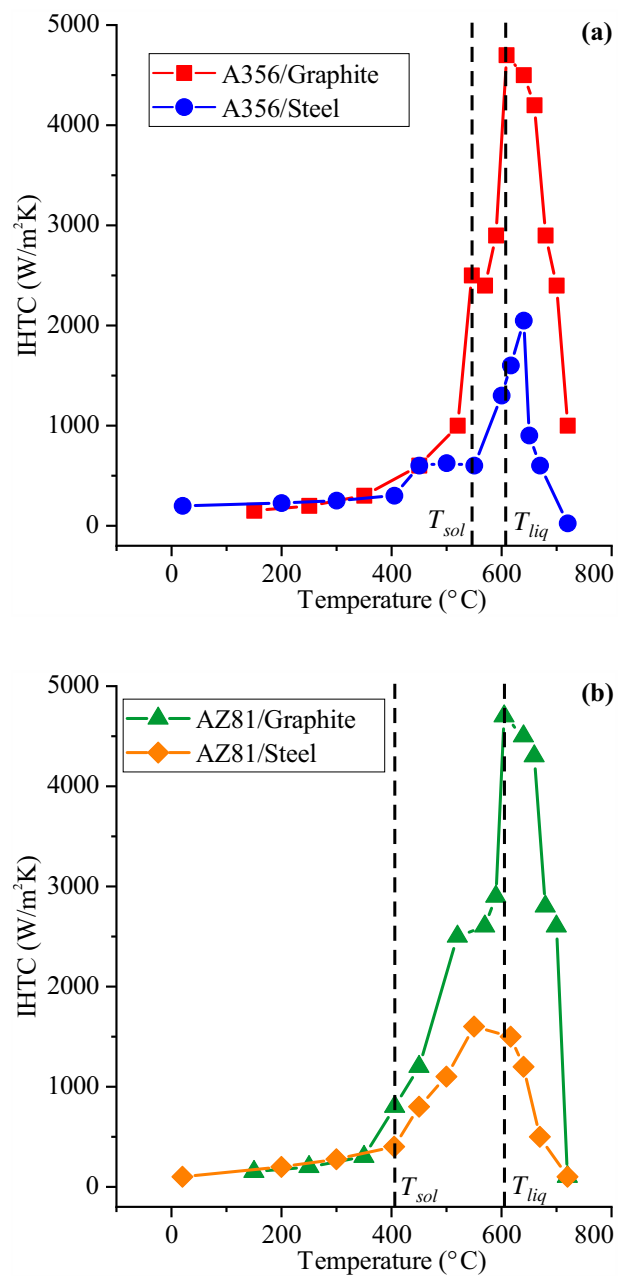


Figure 6. IHTC vs. ingot surface temperature for alloy and mold couples: (a) A356/graphite and A356/steel and (b) AZ81/graphite and AZ81/steel.

Figure 6b shows the IHTC for the AZ81 magnesium alloy and steel mold. The curve for AZ81/steel is much smoother than that for A356/steel. The maximum IHTC of $1600 \text{ W m}^{-2} \text{ K}^{-1}$ was observed near the liquidus temperature of the alloy (608°C). During solidification, the IHTC changes from 1600 to $400 \text{ W m}^{-2} \text{ K}^{-1}$. The peak value of the IHTC at the AZ91/steel mold interface in the literature is twice as high as that found in our work.³⁴ After solidification, the IHTC changed only slightly, and its values were close to those obtained for the A356 alloy and both molds.

The IHTC curves for the AZ81/graphite pair were very similar to those for the A356/graphite pair. The peak IHTC for the AZ81 alloy and graphite mold was $4700 \text{ W m}^{-2} \text{ K}^{-1}$ at the liquidus temperature of the AZ81 magnesium alloy ($608 \text{ }^\circ\text{C}$). The only difference arose at the temperature where the IHTC remained nearly constant because of the lower solidus temperature of the AZ81 alloy. There is no information about the IHTC between magnesium alloys and graphite molds in the literature. Otherwise, the IHTC values found in our work are comparable with those published previously.

A comparison of the curves obtained in our work shows that the IHTCs differed for the steel and graphite molds. The peak IHTC between the ingot and graphite mold was 2–3 times higher than that between the ingot and steel mold, independent of the alloys used. If the ingot surface temperature was lower than the solidus temperature of the alloy, the IHTC for casting into a graphite mold or a steel mold did not differ. After the ingot started to solidify, the IHTC decreased due to shrinkage of the ingot solid skin and expansion of the mold material. The coefficient of thermal expansion (CTE) is the same for A356 and AZ81 alloys with values of 22.5 and $25 \text{ } \mu\text{m m}^{-1} \text{ K}^{-1}$, respectively.³⁶ The graphite and steel CTEs are 7 and $12 \text{ } \mu\text{m m}^{-1} \text{ K}^{-1}$, respectively.^{46, 56, 57} Thus, the shrinkage of the ingots was the same, but the mold expansion was higher than that of the steel mold by nearly a factor of two. However, the ingot solid skin temperature decreased in the range from $\sim 610 \text{ }^\circ\text{C}$ (the alloy liquidus temperature) to $25 \text{ }^\circ\text{C}$, but the mold was heated only by 50 – $135 \text{ }^\circ\text{C}$ with respect to the mold and alloy material, as will be shown hereafter. This means that the gap between the ingot and mold was mostly dependent on shrinkage of the ingot and must be nearly the same for all alloy/mold pairs. This results in the same IHTC for ingot surface temperatures that were lower than alloy solidus temperatures ($< 400 \text{ }^\circ\text{C}$), as shown in our results.

In the case of different alloy ingots being cast in the same mold material, the differences in the IHTC were observed mostly when the alloy was in a liquid or mushy state. It is known that the solidification range for A356 alloys is lower than that for AZ81 alloys, and thus, the IHTC decreased more sharply for the A356 alloy. This trend can be seen clearly in the case of the steel mold casting. For the graphite mold casting, the IHTC curves appear similar for both alloys.

Comparison of the Calculated and Experimental Temperature Curves

Figure 7 shows the simulated and experimental temperature versus time curves for when the A356 aluminum alloy and AZ81 magnesium alloy were solidifying in the steel molds. The IHTC versus temperature dependences shown

in Figure 6 were used in the simulation. The positions of the thermocouples are shown in Figure 1. Thermocouples T1–T4 provided the mold temperature, while thermocouple T5 provided the ingot temperature. For the A356 alloy ingot cast into a steel mold, the simulation and experimental curves agreed well for the majority of the thermocouples. The worst agreement was for T1, which was only 2 mm from the ingot/mold interface. The deviation between the simulation and experimental temperatures for that thermocouple reached $25 \text{ }^\circ\text{C}$. Moreover, for the AZ81 ingot casting into a steel mold, there was good agreement between the simulation and experimental results for all thermocouples.

The temperature versus time curves for all the thermocouples within the mold were very similar for each alloy ingot casting. After pouring the alloy, the temperature increased to a maximum value and then decreased slowly. The maximum temperatures obtained experimentally and with the simulation for each thermocouple associated with the A356 and for AZ81 ingots cast into the steel mold are shown in Table 2. The agreement between the simulated and experimental maximum temperatures was nearly perfect for the AZ81 alloy ingot casting, but in the case of the A356 alloy ingot casting, the differences for the T1 and T2 thermocouples reached $10 \text{ }^\circ\text{C}$.

The means of the experimental maximum mold temperatures for the A356 alloy and the AZ81 alloy cast into a steel mold differed ($160 \text{ }^\circ\text{C}$ vs. $115 \text{ }^\circ\text{C}$ for A356 and AZ81, respectively). The cooling curve (T5) for the A356 alloy also differed from that for the AZ81 alloy. Figure 7 shows that the ingot made of the AZ81 alloy cooled faster and that there was no effect of heat evolution during solidification. In contrast, a clear freezing plateau for the A356 alloy can be seen. The heats of fusion for the A356 and AZ81 alloys are similar (389 J/g and 373 J/g , respectively).³⁶ However, their room temperature densities are 2.69 g/cm^3 and 1.81 g/cm^3 , respectively.³⁶ This means that the latent heats released during solidification of 1 cm^3 of A356 and AZ81 alloys are 1046 J and 674 J , respectively. Thus, the main reason for the differences between the temperature versus time curves for the two alloys is the differences in the released latent heat.

Figure 8 shows curves for the calculated and experimental temperatures versus time during the solidification of the A356 aluminum alloy and AZ81 magnesium alloy in the graphite mold. The IHTC versus ingot surface temperature curves shown in Figure 6 was used for the ingot casting process simulation. Figure 2 shows the positions of the thermocouples. Thermocouple T5 was in the mold cavity and provided the ingot temperature, while the other thermocouples provided the mold temperatures. The simulation and the experimental results agreed well for most thermocouples for the A356 and AZ81 ingots cast into a graphite mold, but there were some exceptions, specifically for

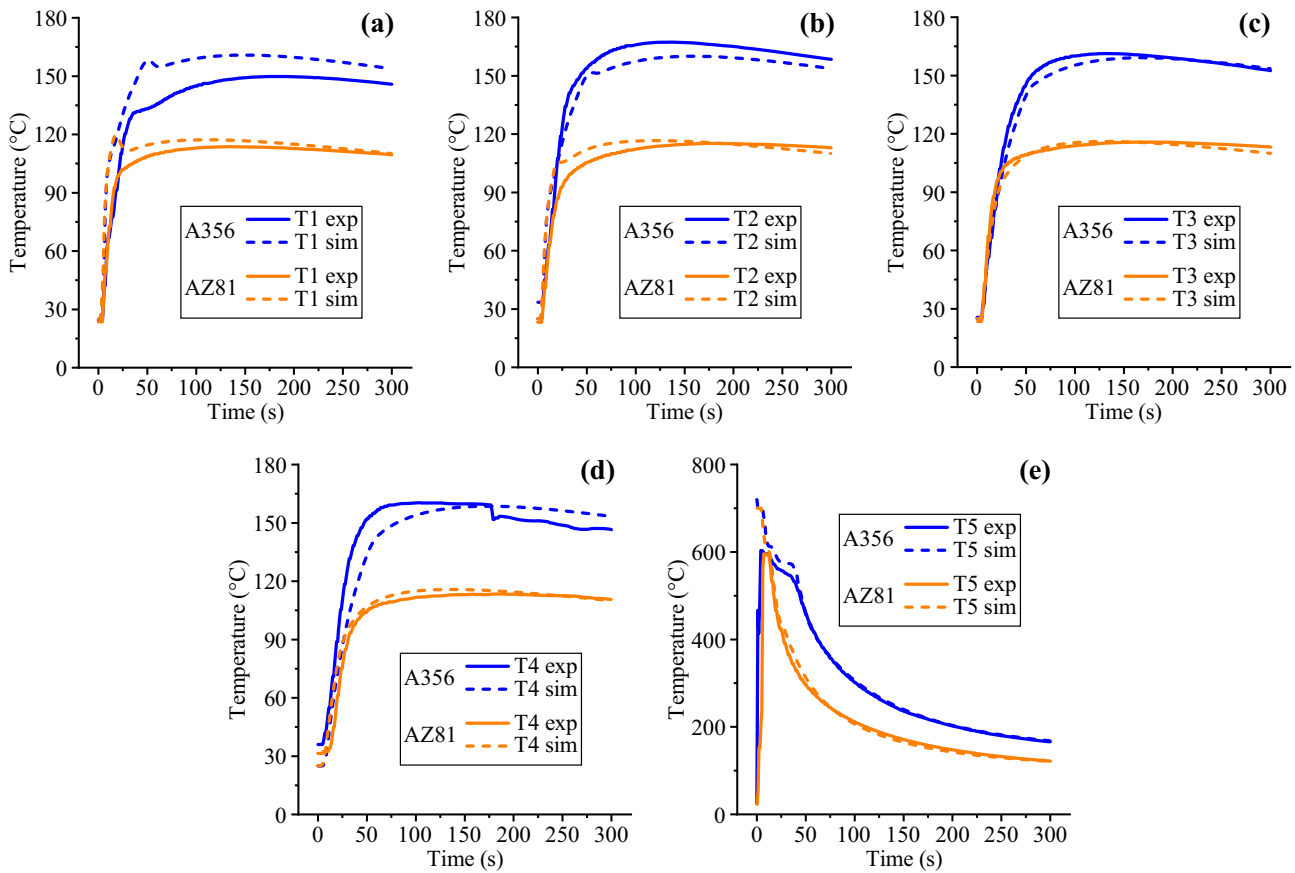


Figure 7. Comparisons of calculated and experimental temperatures for A356 and AZ81 alloys cast into a steel mold: (a) T1, (b) T2, (c) T3, (d) T4, and (e) T5. The positions of the thermocouples are shown in Figure 1.

Table 2. Maximum Temperatures for Thermocouples Placed in the Steel Mold

Thermocouple	A356		AZ81	
	Experimental (°C)	Simulated (°C)	Experimental (°C)	Simulated (°C)
T1	150	161	114	117
T2	167	160	115	117
T3	161	159	116	116
T4	160	159	113	116

thermocouples T2, T6, and T8. For those thermocouples, the deviation between the experimental and simulation results reached 20 °C. For thermocouple T5, no freezing plateau connected with heat evolution during solidification was observed for either alloy. This may be due to the high cooling rate.

The temperature versus time curves obtained for the ingots cast into the graphite molds differed from those obtained for the steel molds. In Table 3, the maximum temperatures obtained experimentally and with the simulations for each thermocouple for the A356 and for AZ81 ingots cast into a graphite mold are shown. The maximum temperature

decreased as the distance from the mold/ingot interface increased. For example, the maximum experimental (simulated) temperature for thermocouple T1, which was 2 mm from the mold cavity, was 190 °C (142 °C), and for thermocouple T4, which was 20 mm from the mold cavity, it was 82 °C (87 °C). The same was observed for the AZ81 ingot casting into a graphite mold. Another difference for the ingot casting in graphite mold as compared to the steel mold is that initially after pouring, the temperature sharply increased to its maximum value and then sharply decreased for thermocouples positioned near the ingot/mold interface. After this decrease, the temperature remained almost constant and the same for all thermocouples. The reason for

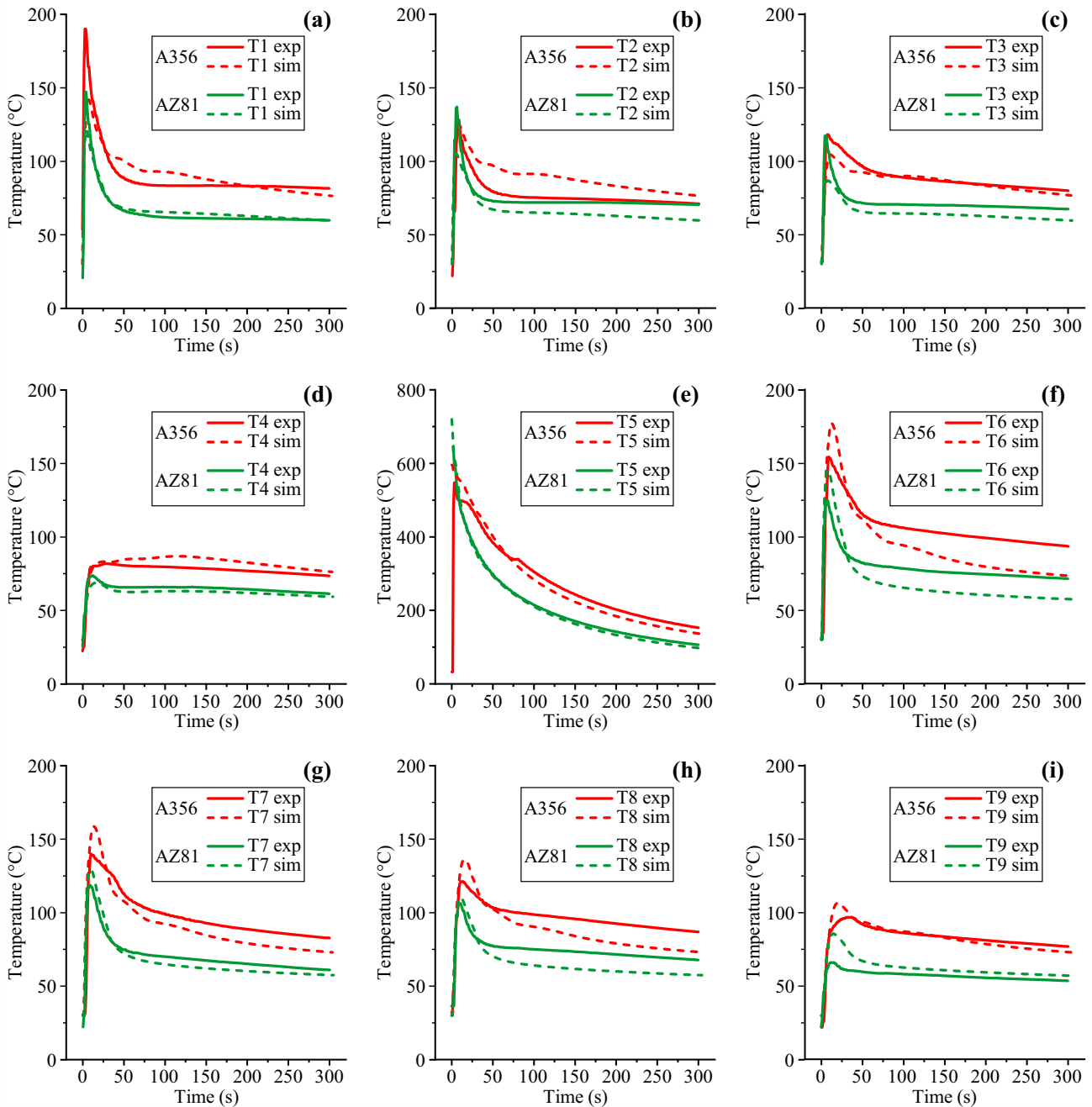


Figure 8. Comparison of calculated and experimental temperatures for the A356 and AZ81 alloys cast into a graphite mold: (a) T1, (b) T2, (c) T3, (d) T4, (e) T5, (f) T6, (g) T7, (h) T8, and (i) T9. The positions of the thermocouples are shown in Figure 2.

this discrepancy between the thermal profiles for the steel and the graphite molds is the higher IHTC for the alloy/graphite pair. In the first seconds after pouring, there was a large amount of heat absorbed by the mold, and a thin mold layer in good contact with the melt was heated to temperatures up to ~ 200 °C. It can be seen that the graphite thermal conductivity was two times higher than that of steel (Figure 5), but it was still not enough to flatten the mold temperature profile.

In the case of the graphite mold castings, the thermocouples in the mold were positioned at two different heights. Thermocouples T1–T4 were at the lower level, and thermocouples T6–T9 were at the higher level. It can be seen that the experimental maximal temperatures were higher than the simulated temperatures for the lower levels for both the A356 and AZ81 alloy ingot castings. The opposite was observed for the thermocouples at the higher level, where the experimental maximal temperatures were lower than the simulated maximal temperatures. The same results were obtained previously when pure aluminum was cast

Table 3. Maximum Temperatures for Thermocouples Placed in the Graphite Mold

Thermocouple	A356		AZ81	
	Experimental °C	Simulated °C	Experimental °C	Simulated °C
T1	190	142	147	122
T2	128	125	137	105
T3	118	104	117	87
T4	82	87	74	69
T6	154	177	125	145
T7	140	159	119	129
T8	121	136	106	110
T9	97	107	66	86

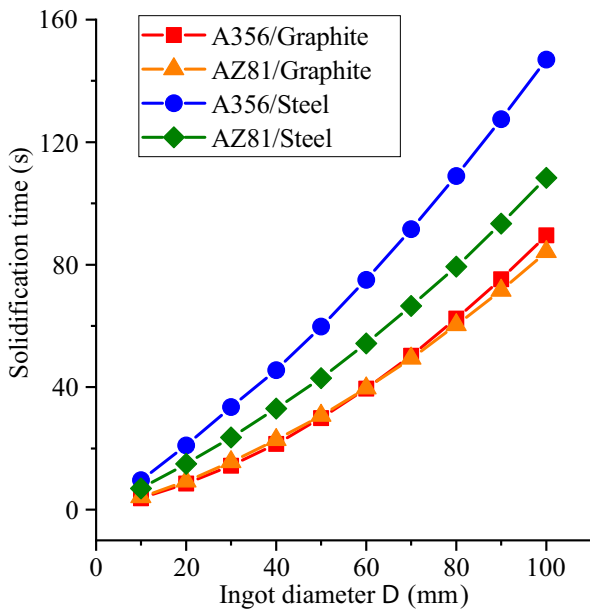


Figure 9. Solidification time vs. ingot diameter for the different alloy/mold couples.

into a graphite mold.⁴³ The IHTC varied over the ingot height because the metallostatic pressure and plasticity of the solidified ingot skin affected the air gap between the metal and mold.⁵⁸

Comparison of the Solidification Times and Cooling Rates for Ingots in the Steel Molds and Graphite Molds

Figure 9 presents the ingot solidification time versus ingot diameter for the different alloy/mold couples. In the steel mold, the solidification times for the A356 alloy ingot were higher than those for the AZ81 alloy ingot. For example, for an ingot diameter $D = 100$ mm, the solidification times for the A356 and AZ81 alloys in the steel mold were 147

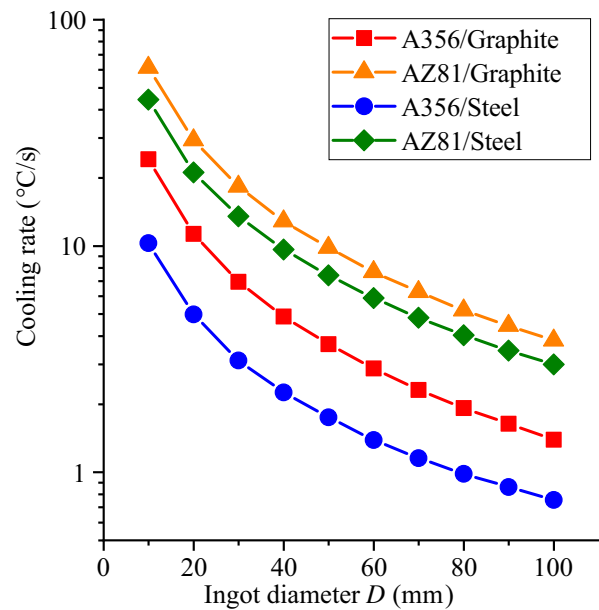


Figure 10. Cooling rate vs. ingot diameter for the different alloy/mold couples.

and 108.3 s, respectively. As shown previously, more heat was released during solidification of the A356 alloy than during AZ81 alloy solidification. However, in the graphite mold, the solidification times for A356 were almost the same as those for AZ81 for all diameters. They changed from 3.7 to 4.1 s at $D = 10$ mm to 89.6–84.2 s at $D = 100$ mm. This means that during solidification of the alloy in the graphite mold, all of the heat released during A356 alloy solidification was absorbed faster by the graphite mold than by the steel mold.

As expected, the solidification times for all ingot diameters were higher for the steel molds. The largest differences between the solidification times for the A356 ingot with $D = 100$ mm in the steel and graphite molds were 147 s and 89.6 s, respectively. The lower solidification time for

the ingots in the graphite mold was due to the higher IHTC between the alloy/graphite interface than that between the alloy/steel interface.

The simulated cooling rates during solidification versus the ingot diameter for different alloy/mold material couples are shown in Figure 10. For the A356 ingot at diameter $D = 10$ mm, the cooling rate of the ingot solidified in the steel mold was 10.3 °C/s, and for the ingot solidified in the graphite mold, it was 24.2 °C/s. With increasing ingot diameter to $D = 100$ mm, the cooling rates were 0.8 °C/s in the steel mold and 1.4 °C/s in the graphite mold. Thus, the cooling rates for the graphite mold were nearly twice as high as those of the steel mold. As the ingot diameter increased, the differences in the cooling rate decreased. As we can see, the cooling rates were higher for the AZ81 ingot in both the steel and graphite molds. At ingot diameter $D = 10$ mm for the AZ81 alloy, the cooling rates of the ingot in the steel mold and the graphite mold were 44.4 and 61.4 °C/s, respectively. For the largest diameter $D = 100$ mm, the cooling rates in the steel mold and the graphite mold were 3.0 and 3.8 °C/s, respectively. In other words, the difference between the cooling rates for the AZ81 alloy ingot in a steel mold and a graphite mold was only $\sim 25\%$, regardless of the ingot diameter. This was due to the lower latent heat released during AZ81 alloy solidification in comparison with that for the A356 alloy. For both alloys, the cooling rates were higher in the graphite mold, which was related to the higher IHTC for the alloy/graphite surface than that for the alloy/steel surface.

Conclusions

- (1) The IHTC versus ingot surface temperature dependences were found for ingots of alloys A356 and AZ81 during solidification in steel and graphite molds. The peak IHTC values at the metal/mold interface for the A356 alloy ingot cast into a steel mold and into a graphite mold were 2050 and 4700 $\text{W m}^{-2} \text{K}^{-1}$, respectively. For the AZ81 alloy ingot cast into a steel mold and into a graphite mold, the peak IHTC values were 1600 and 4700 $\text{W m}^{-2} \text{K}^{-1}$, respectively.
- (2) There was a good fit between the simulated temperature profiles calculated using the IHTC values obtained in our work and the experimental temperature profiles. Note that when casting into steel molds, the temperature versus time curves for thermocouples at different distances from the ingot/mold interface were nearly identical. In contrast, when casting into graphite molds, the maximum temperatures for thermocouples closer to the ingot/mold surface were higher than those for thermocouples farther from the ingot/mold surface.

- (3) The solidification times for the A356 alloy ingots in steel molds were nearly twice as long as those for graphite molds for both small (10 mm) and large (100 mm) ingot diameters. The differences in the solidification times of the ingots in the steel and graphite molds were lower for the AZ81 alloy than for the A356 alloy. For the A356 and AZ81 ingots, the solidification times in the graphite molds were the same but differed for the steel molds.
- (4) The cooling rates for the A356 alloy in the steel molds were nearly half those for the graphite molds for both small (10 mm) and large (100 mm) diameters. However, the differences in the cooling rates for the AZ81 alloy for both types of molds were smaller. The cooling rates for the graphite molds were nearly 1.4 times those for the steel molds with diameters of 10 and 100 mm.

Acknowledgements

This research received financial support from the Ministry of Science and Higher Education in the Russian Federation (Agreement No. 075-11-2019-045 from 22 November 2019) under the program “Scientific and technological development of the Russian Federation” according to governmental decree N 218 dated 9 April 2010.

Compliance with Ethical Standards

Conflict of interest No potential conflict of interest was reported by the authors.

REFERENCES

1. P. Sharifi, Y. Fan, H.B. Anaraki et al., *Met. Mater. Trans. A*, **47**, 5159 (2016). <https://doi.org/10.1007/s11661-016-3698-x>
2. N.A. Belov, A.N. Alabin, A.Yu. Prokhorov, *Russ. J. Non-Ferr. Met.* **50**, 357 (2009). <https://doi.org/10.3103/S1067821209040099>
3. N.A. Belov, A.N. Alabin, I.A. Matveeva, *J. Alloy. Compd.* **583**, 206 (2014). <https://doi.org/10.1016/j.jallcom.2013.08.202>
4. S. O'Connor, *Adv. Mater. Process.* **166**, 29 (2008)
5. S. O'Connor, *AMMTIAC Quart.* **2**, 3 (2007)
6. L. Jia, D. Xu, M. Li, J. Guo, H. Fu, *Met. Mater. Int.* **18**, 55 (2012). <https://doi.org/10.1007/s12540-012-0007-0>
7. V. Zanchuk, *Adv. Mater. Process.* **162**, 66 (2004)
8. V. Zanchuk, *Die Cast. Eng.* **1**, 38 (2006)
9. G.V. Mysov, *Chem. Petrol. Eng.* **11**, 1038 (1975). <https://doi.org/10.1007/BF01152456>
10. G. Baumeister, D. Buqezzi-Ahmeti, J. Glaser, H.-J. Ritzhaupt-Kleissl, *Microsyst. Technol.* **17**, 289 (2011). <https://doi.org/10.1007/s00542-011-1237-7>

11. W.C. Chen, F.Y. Teng, C.C. Hung, *Mater. Sci. Eng., C* **35**, 231 (2014). <https://doi.org/10.1016/j.msec.2013.11.014>
12. A.Y.C. Nee, *Handbook of Manufacturing Engineering and Technology* (Springer, London, 2015)
13. K.N. Prabhu, K.M. Suresha, *J. Mater. Eng. Perform.* **13**, 619 (2004). <https://doi.org/10.1361/10599490420647>
14. K.N. Prabhu, W.D. Griffiths, *Mater. Sci. Forum* **329**, 455 (2000). <https://doi.org/10.4028/www.scientific.net/MSF.329-330.455>
15. D. Wang, C. Zhou, G. Xu, A. Huaiyuan, *J. Mater. Process. Technol.* **214**, 1275 (2014). <https://doi.org/10.1016/j.jmatprotec.2014.01.009>
16. W.D. Griffiths, K. Kawai, *J. Mater. Sci.* **45**, 2330 (2010). <https://doi.org/10.1007/s10853-009-4198-9>
17. Z. Sun, H. Hu, X. Niu, *J. Mater. Process. Technol.* **211**, 1432 (2011). <https://doi.org/10.1016/j.jmatprotec.2011.03.014>
18. Y. Nishida, W. Droste, S. Engler, *Metall. Mater. Trans. B* **17**, 833 (1986). <https://doi.org/10.1007/BF02657147>
19. D. Bouchard, S. Leboeuf, J.P. Nadeau, R.I.L. Guthrie, M. Isac, *J. Mater. Sci.* **44**, 1923 (2009). <https://doi.org/10.1007/s10853-008-2888-3>
20. A. Prasad, I.F. Bainbridge, *Metall. Mater. Trans. A* **44**, 3099 (2013). <https://doi.org/10.1007/s11661-013-1646-6>
21. S.L. Lu, F.R. Xiao, S.J. Zhang, Y.W. Mao, B. Liao, *Appl. Therm. Eng.* **73**, 512 (2014). <https://doi.org/10.1016/j.applthermaleng.2014.07.073>
22. K.N. Prabhu, B. Chowdary, N. Venkataraman, *J. Mater. Eng. Perform.* **14**, 604 (2005). <https://doi.org/10.1361/105994905X66015>
23. L. Chen, Y. Wang, L. Peng, P. Fu, H. Jiang, *Exp. Therm. Fluid Sci.* **54**, 196 (2014). <https://doi.org/10.1016/j.expthermflusci.2013.12.010>
24. G. Palumbo et al., *Appl. Therm. Eng.* **78**, 682 (2015). <https://doi.org/10.1016/j.applthermaleng.2014.11.046>
25. F. Bertelli, N. Cheung, A. Garcia, *Appl. Therm. Eng.* **61**, 577 (2013). <https://doi.org/10.1016/j.applthermaleng.2013.08.034>
26. M.A. Martorano, J.D.T. Capocchi, *Int. J. Heat Mass Transfer.* **43**, 2541 (2000). [https://doi.org/10.1016/S0017-9310\(99\)00298-7](https://doi.org/10.1016/S0017-9310(99)00298-7)
27. W.D. Griffiths, *Metall. Mater. Trans. B* **31**, 285 (2000). <https://doi.org/10.1007/s11663-000-0047-6>
28. J. Kron, T. Antonsson, H. Fredriksson, *Int. J. Cast Met. Res.* **14**, 275 (2002). <https://doi.org/10.1080/13640461.2002.11819445>
29. N. Akar, H.M. Şahin, N. Yalçın, K. Kocatepe, *Exp. Heat Transfer.* **21**, 83 (2008). <https://doi.org/10.1080/08916150701647785>
30. J.A. Hines, *Metall. Mater. Trans. B* **35**, 299 (2004). <https://doi.org/10.1007/s11663-004-0031-7>
31. J. Swan, M. Ward, R.C. Reed, *Mater. Sci. Forum* **765**, 276 (2013). <https://doi.org/10.4028/www.scientific.net/MSF.765.276>
32. M. Trovant, S.A. Argyropoulos, *Can. Metall. Q.* **37**, 185 (1998). <https://doi.org/10.1179/cm.1998.37.3-4.185>
33. A.S. Sabau, *Int. J. Cast Met. Res.* **19**, 188 (2006). <https://doi.org/10.1179/136404606225023390>
34. J.H. Kuo, R.J. Weng, W.S. Hwang, *Mater. Trans.* **47**, 2547 (2006). <https://doi.org/10.2320/matertrans.47.2547>
35. M.A. Taha, N.A. El-Mahallawy, M.T. El-Mestekawi, A.A. Hassan, *Mater. Sci. Technol.* **17**, 1093 (2001). <https://doi.org/10.1179/026708301101511004>
36. *ASM International Handbook Committee, ASM Handbook, Properties and Selection: Nonferrous Alloys and Special-Purpose Materials*, tenth ed., Vol. 2. (ASM International, Materials Park, 2002), pp. 624–1546
37. A.Yu. Kachalov, V.D. Belov, V.E. Bazhenov, A.V. Fadeev, *Tsvetnye Metally.* **2019**, 84 (2019). <https://doi.org/10.17580/tsm.2019.06.12>
38. ESI Group, ProCAST 2010.0 User's Manual (ESI Group, 2010), https://myesi.esi-group.com/system/files/documentation/ProCAST/2010/ProCAST_20100_UM.pdf. Accessed 1 August 2019
39. L. Yang et al., *Intermetallics* **66**, 149 (2015). <https://doi.org/10.1016/j.intermet.2015.07.006>
40. S.L. Lu et al., *Appl. Therm. Eng.* **93**, 518 (2016). <https://doi.org/10.1016/j.applthermaleng.2015.09.114>
41. J.A. Dantzig, M. Rappaz, *Solidification* (EPFL Press, Lausanne, 2009), pp. 105–151
42. E.I. Zhmurikov, I.V. Savchenko, S.V. Stankus, O.S. Yatsuk, L.B. Tecchio, *Nucl. Instr. Meth. Phys. Res. A.* **674**, 79 (2012). <https://doi.org/10.1016/j.nima.2012.01.015>
43. V.E. Bazhenov, A.V. Koltygin, Yu.V. Tselovalnik, A.V. Sannikov, *Russ. J. Non Ferr. Met.* **58**, 114 (2017). <https://doi.org/10.3103/S1067821217020031>
44. R.D. Pehlke, A. Jeyarajan, H. Wada, Summary of thermal properties for casting alloys and mold materials. *STIN* **83**, 36293 (1982)
45. P.A. Schweitzer, *Metallic Materials: Physical, Mechanical, and Corrosion Properties* (Marcel Dekker Inc, New York, 2003). <https://doi.org/10.1201/9780203912423>
46. *ASM International Handbook Committee, ASM Handbook, Properties and selection: Irons, steels and high performance alloys*, Vol. 1, tenth ed., (ASM International, Materials Park, 1990)
47. R.E. Taylor, H. Groot, *Thermophysical Properties of POCO Graphite* (Purdue University, West Lafayette, IN, 1978), p. 16
48. A.I. Bencomo, R.I. Bisbal, R. Morales, *Revista Materia* **13**, 294 (2008). <https://doi.org/10.1590/S1517-70762008000200007>

49. S.I. Bakhtiyarov, R.A. Overfelt, S.G. Teodorescu, J. Mater. Sci. **36**, 4643 (2001). <https://doi.org/10.1023/A:1017946130966>
50. K.O. Yu, *Modeling for Casting and Solidification Processing* (CRC Press, New York, 2001)
51. A. Lindemann, J. Schmidt, M. Todte, T. Zeuner, Thermochem. Acta **382**, 269 (2002). [https://doi.org/10.1016/S0040-6031\(01\)00752-3](https://doi.org/10.1016/S0040-6031(01)00752-3)
52. A. Rudajevová, M. Staněk, P. Lukáč, Mater. Sci. Eng., A **341**, 152 (2003). [https://doi.org/10.1016/S0921-5093\(02\)00233-2](https://doi.org/10.1016/S0921-5093(02)00233-2)
53. S. Lee, H.J. Ham, S.Y. Kwon, S.W. Kim, C.M. Suh, Internat. J. Thermophys. **34**, 2343 (2013). <https://doi.org/10.1007/s10765-011-1145-1>
54. A. Rudajevová, P. Lukáč, Acta Universitatis Carolinae. Mathematica et Physica. **41**, 3 (2000)
55. A. Rudajevová, J. Kiehn, K.U. Kainer, B.L. Mordike, P. Lukáč, Scripta Mater. **40**, 57 (1998). [https://doi.org/10.1016/S1359-6462\(98\)00390-X](https://doi.org/10.1016/S1359-6462(98)00390-X)
56. A.L. Pinter, Carbon **9**, 637 (1971). [https://doi.org/10.1016/0008-6223\(71\)90086-8](https://doi.org/10.1016/0008-6223(71)90086-8)
57. S. Bidhar, N. Simos, D. Senor, P. Hurh, Nucl. Mater. Energy. **24**, 100761 (2020). <https://doi.org/10.1016/j.nme.2020.100761>
58. N.A. El-Mahallawy, A.M. Assar, J. Mater. Sci. Lett. **7**, 205 (1988). <https://doi.org/10.1007/BF01730171>

Publisher's Note Springer Nature remains neutral with regard to jurisdictional claims in published maps and institutional affiliations.